Prediction of Health Level of Multiform Lithium Sulfur Batteries Based on Incremental Capacity Analysis and an Improved LSTM

Hao Zhang, Hanlei Sun, Le Kang, Yi Zhang, Licheng Wang, and Kai Wang

***Abstract*—Capacity estimation plays a crucial role in battery management systems, and is essential for ensuring the safety and reliability of lithium-sulfur (Li-S) batteries. This paper proposes a method that uses a long short-term memory (LSTM) neural network to estimate the state of health (SOH) of Li-S batteries. The method uses health features extracted from the charging curve and incremental capacity analysis (ICA) as input for the LSTM network. To enhance the robustness and accuracy of the network, the Adam algorithm is employed to optimize specific hyperparameters. Experimental data from three different groups of batteries with varying nominal capacities are used to validate the proposed method. The results demonstrate the effectiveness of the method in accurately estimating the capacity degradation of all three batteries. Also, the study examines the impact of different lengths of network training sets on capacity estimation. The results reveal that the ICA-LSTM model achieves a prediction accuracy of mean absolute error 4.6% and mean squared error 0.21% with three different training set lengths of 20%, 40%, and 60%. The analysis demonstrates that the lightweight model maintains high SOH estimation accuracy even with a small training set, and exhibits strong adaptive and generalization capabilities when applied to different Li-S batteries. Overall, the proposed method, supported by experimental validation and analysis, demonstrates its efficacy in ensuring accurate and reliable SOH estimation, thereby enhancing the safety and performance of Li-S batteries.**

***Index Terms*—Adam algorithm, incremental capacity analysis, Li-S battery, long short-term memory, state of health.**

I. Introduction

There is now a significant emphasis on the development of sustainable energy and reduction of environment pollution. To achieve this, it is essential to reduce the reliance on fossil fuels and strive for a transition to clean, renewable energy sources such as solar and wind. Nevertheless, the intermittent nature of renewable energy necessitates the integration of advanced energy storage systems capable of efficiently capturing renewable energy and delivering it when required [1]–[4]. Battery systems can play a key role in these areas as an efficient intermediary for storing and releasing energy. However, lithium-ion (Li-ion) batteries commonly used in small portable electronic devices cannot meet the high energy demand of stationary grid energy storage [5]–[7], whereas their low energy density also hinders their application in emerging mobile transportation devices, such as electric vehicles [8], [9]. Compared with gasoline vehicles, electric vehicles are more environmentally friendly and safer. This has prompted research in developing better and more efficient battery energy systems [10]–[12].

Recently, research on the lithium-sulfur (Li-S) battery has attracted extensive attention. The electrochemical reaction mechanisms of Li-S and Li-ion batteries are different [13]. Lithium-ion intercalation in layered electrode materials (such as graphite anode and lithium metal oxide cathode) in Li-ion batteries is often only able to intercalate into some specific sites, and the energy density is usually 420 Wh/kg [14]. In contrast, Li-S battery offers a high theoretical specific capacity (1675 Wh/kg) and energy density (2600 Wh/kg), while the sulfur element is both cost-effective and readily available, making Li-S batteries one of the attractive next-generation low-cost energy storage technologies [15]–[18]. Li-S batteries are mainly composed of positive electrodes, electrolytes, separators, and negative electrodes [19]. Their cathode material, sulfur, is a crown structure composed of eight sulfur atoms, and has very stable thermodynamic properties [20]. The high charge-discharge performance of sulfur is related to the cleavage and reorganization of sulfur-sulfur bonds in the S8 molecule [21]–[23]. However, at present, Li-S batteries have problems such as rapid capacity decay,

Received: April 18, 2023
Accepted: October 31, 2023
Published Online: March 1, 2024
Kai Wang (corresponding author) is with the School of Electrical Engineering, Qingdao University, Qingdao 266000, China (e-mail: wangkai@qdu. edu.cn).
Hanlei Sun (corresponding author) is with the School of Electrical Engineering, Qingdao University, Qingdao 266000, China (e-mail: 2020025742@qdu.edu.cn).
DOI: 10.23919/PCMP.2023.000280

low conductivity of the sulfur cathode, polysulfide "shuttle effect", deposition of lithium ions, and volume change induced-structural changes during charge and discharge. Consequently, it is difficult to achieve large-scale commercial production [24]–[26].

In addition, to commercialize Li-S batteries, various technological challenges must be addressed. This paper seeks to address one of these challenges: state of health (SOH) estimation of Li-S batteries. SOH is an important part of battery management systems (BMS) as it plays a vital role in ensuring the safe and efficient operation of batteries. This aspect is particularly essential for batteries that are intended for large-scale deployment and is also valuable for end-users [27].

Numerous studies have proposed a variety of approaches to develop battery SOH estimates, which can be broadly divided into three categories: model-based, data-driven, and hybrid methods that combine the first two approaches [28]–[32]. A method based on the use of forgetting factor recursive least squares was proposed to identify the equivalent circuit model, which is combined with support vector machine classification to complete the estimation of Li-S battery SOH [33]. Reference [34] proposes an SOH model based on capacity and power fading, and a double extended Kalman filter is used to estimate the SOH of Li-S batteries. In [35], a joint estimation model based on incremental capacity analysis and a bidirectional long short-term memory (Bi-LSTM) neural network is proposed to estimate the SOH of Li-ion batteries, whereas a method using empirical mode decomposition (EMD) to noise-combined multi-kernel correlation vector machine method is proposed for Li-ion battery SOH prediction in [36]. Reference [37] proposes an improved robust multi-time scale singular filtering-Gaussian process regression-long short-term memory (SF-GPR-LSTM) modeling method for the remaining capacity estimation, while an improved anti-noise adaptive long short-term memory (ANA-LSTM) neural network with high-robustness feature extraction and optimal parameter characterization is proposed for accurate remaining useful life (RUL) prediction [38].

Based on the experimental results of the previously proposed method, it is evident that the model-based method can achieve higher accuracy for a certain category of batteries. However, it still has limitations when it comes to nonlinear system planning and the identification and prediction of batteries across multiple categories. In other words, it lacks robustness and generalizability. On the other hand, the deep learning method, while consuming certain computational resources, manages to maintain high accuracy and strong generalizability simultaneously. For Li-S batteries, the existing methods only include model-based methods, with the field of data-driven deep learning remaining unexplored. This, in turn, underscores the significance and novelty of our research.

Because of the widespread commercialization of Li-ion batteries, numerous methods have been proposed to estimate the aging states. However, it is important to note that the internal reactions of Li-ion batteries differ significantly from those of Li-S batteries. In addition, the nonlinear decay process also varies. Consequently, the conventional Li-ion battery SOH model is inadequate for Li-S batteries. Therefore, it is important to develop an accurate and applicable SOH estimation method for Li-S batteries. This will not only enhance the understanding of battery aging but also serve as a crucial prerequisite for the large-scale implementation of Li-S batteries, ensuring their performance and stability.

The existing SOH prediction methods for Li-S batteries are primarily model-based estimation approaches, such as the Kalman filter and least squares methods. These methods are heavily dependent on accurate modeling of the batteries. However, they also require frequent parameter identification and replacement of equivalent topology models when the battery internal characteristics change. This process consumes significant resources and requires iterative detection and estimation, leading to only average computational efficiency. To address these limitations, this paper proposes a novel SOH estimation method for Li-S batteries based on incremental capacity analysis (ICA) and deep learning models. Deep learning, as a data-driven algorithm, eliminates the need for extensive modeling efforts, while it focuses on identifying features highly correlated with battery capacity degradation. The ICA method is employed to extract features from the incremental capacity (IC) curve after Savitzky-Golay (SG) filtering. The features exhibit a strong correlation with battery capacity decay. They are then combined with conventional battery charging and discharging features to create a comprehensive feature map, which is subsequently input into a long short-term memory (LSTM) model for Li-S battery SOH estimation. To validate the accuracy and generalizability of the proposed method, transfer learning techniques are applied. The results underscore the innovative and forward-thinking nature of the method, as it attains high accuracy and demonstrates strong generalizability. By introducing a data-driven approach and leveraging the power of deep learning, this research marks a significant departure from the traditional model-based methods used in SOH prediction for Li-S batteries. The proposed method not only reduces the computational burden associated with parameter identification and model replacement but also demonstrates its superior accuracy and generalizability, paving the way for future advances.

The rest of the paper is arranged as follows. Section II introduces the characteristics of Li-S batteries and the

processing of charge and discharge data. Section III introduces ICA and feature extraction, while Section IV analyzes the methodology in detail. Section V conducts example analysis, establishes the Li-S battery SOH estimation model and performs multi-dataset verification. Section VI summarizes the contributions of this paper.

II. Data Processing of Li-S Battery

The Li-S batteries used in this study use carbon coating materials to suppress the shuttle effect of polysulfides, while interconnected carbon nanocages are used as the coating material for the separator of Li-S batteries. As for the commercial separators used to expand the data set, they refer to graphite separators. Physical barriers are used to inhibit the shuttling of lithium polysulfide, while high conductivity and high specific surface area also help to reduce local current density and improves uniformity of lithium-ion deposition. The platform shown in Fig. 1 is used to perform cyclic charge-discharge tests and data collection [39]. The Li-S battery has excellent electrochemical performance at different rates, and the rest of the battery information is shown in Table I. It is worth noting that because of the randomness of the experiments and the need to verify the generalizability of the model, the maximum capacity of the Li-S battery tested by electrochemical workstations with different rates fluctuates between 1.3–1.6 Ah, while the range of charging voltage and the value of charging current and temperature are the same.

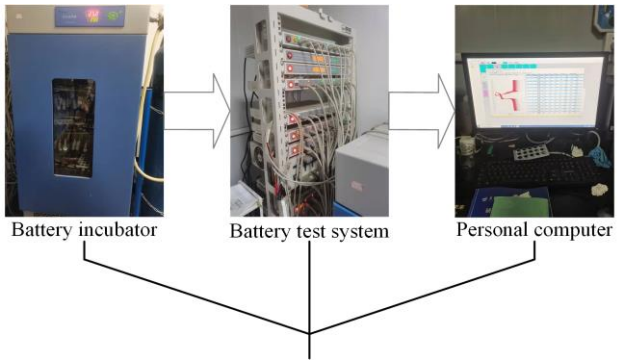

Fig. 1. Li-S battery test platform.

TABLE I
Li-S Battery Information

Designation	Norm
Rated capacity (mAh)	0.5–1
Material	S/Li
Voltage range (V)	1.7–2.6
Charge/discharge current (A)	0.422
Temperature (°C)	25

The voltage curve and capacity decay curve of the Li-S battery used at three charge-discharge rates of 1 C, 0.5 C, and 0.2 C are shown in Fig. 2. Because of the change of the charge rate, the single-cycle charge-discharge time also changes, but the features that can be captured are very similar. These are the basis for using deep learning to build the SOH model of Li-S batteries. However, as shown in Fig. 2(d), the capacity decay curves under the three charging rates are nonlinear, while the first 10 cycles are used as the test interval and are not used in the training of the model. As an indicator of the degree of battery deterioration, its SOH is not clearly defined. It is generally believed that the SOH can be calculated by the ratio of the current maximum capacity to the initial capacity, expressed as:

$$SOH = \frac{C_t}{C_0} \tag{1}$$

where C_t is the current remaining capacity of the battery; and C_0 is the rated capacity.

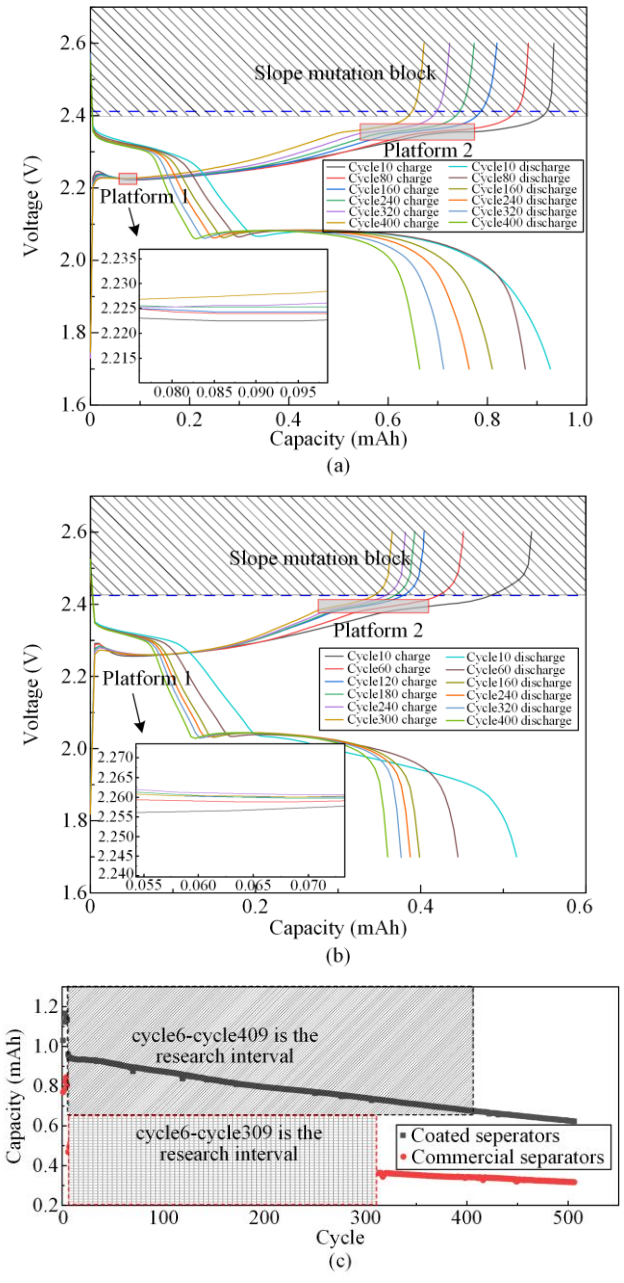

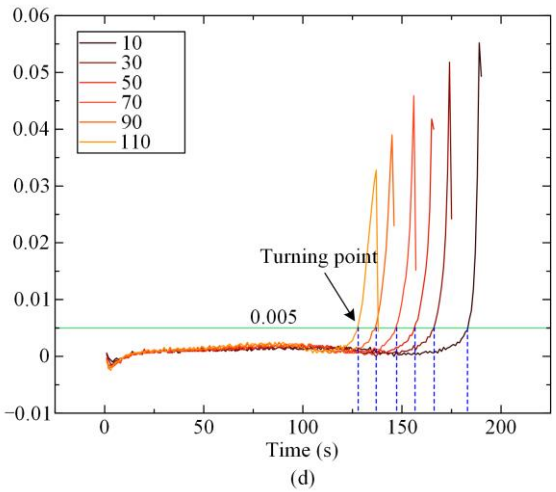

Fig. 2. The voltage curve and capacity decay curve of the Li-S battery used at three charge-discharge rates of 1 C, 0.5 C, and 0.2 C. (a) Li-S battery voltage-capacity curves of coated separators. (b) Li-S battery voltage-capacity curve for commercial separators. (c) Capacity decay curves of two Li-S batteries. (d) Charge voltage full differential curve.

III. Feature Extraction

A. Charging Voltage Feature Extraction

The health feature is an indicator to describe the aging degree of the Li-S battery during the cycle of charge and discharge. Accurately capturing the feature is a necessary condition for training an accurate battery SOH prediction model. The charging and discharging process of the Li-S battery is given as follows:

Negative reaction:

$$\mathrm{Li} \leftrightarrow \mathrm{Li}^+ + \mathrm{e}^- \tag{2}$$

$$\mathrm{Li_2S_n} + \mathrm{Li} \rightarrow \mathrm{Li_2S_m} \cdots\cdots (3 \leqslant m < n \leqslant 8) \tag{3}$$

Positive reaction:

$$\mathrm{S_8} + \mathrm{Li}^+ + \mathrm{e}^- \leftrightarrow \mathrm{Li_2S_n} \cdots\cdots (3 \leqslant n \leqslant 8) \tag{4}$$

$$\mathrm{Li_2S_m} + \mathrm{Li}^+ + \mathrm{e}^- \leftrightarrow \frac{\mathrm{Li_2S_2}}{\mathrm{Li_2S}} \tag{5}$$

The general reaction formula of a Li-S battery is: $\mathrm{S_8} + 16\mathrm{Li} = 8\mathrm{Li_2S}$.

It can be seen from the positive and negative reactions that the Li-S battery is a continuous multi-electron redox process. Figure 2(c) shows the capacity decay cycle of the selected commercial separators and coated separators batteries, while the gray box is the stage of capacity decay from brand new to end of life. From Figs. 2 (a) and (b), there are two platforms in the charging process of the Li-S battery, i.e., the charging Platform 1 is around 2.2 V, and the charging Platform 2 is around 2.3 V. The redox reactions that occur intensively in these two processes lead to the emergence of voltage plateaus, which will be explained in detail in the following sections. In addition, the internal reaction of the battery also leads to a sharp increase in the charging voltage slope near 2.4 V, and as the number of cycles increases, this interval gradually shifts to the right and is closely related to the decreasing trend of capacity. Therefore, the voltage value corresponding to the voltage inflection point is chosen as the first input feature to extract the voltage inflection point and obtain the full differential of the charging voltage curve, as shown in Fig. 2. Because of the sudden change in the slope during each cycle when the voltage reaches approximately 2.4 V, a line is drawn with a slope of 0.005 and the intersection of each total differential curve is extracted as the voltage turning point.

B. Incremental Capacity Analysis

ICA can deeply explore and quantitatively analyze the dynamic relationship between voltage and capacity during battery charging and discharging. The previous section has described the two voltage platforms between 2.3 V and 2.2 V. At this point, the redox reaction reaches a high equilibrium. The internal voltage of the battery changes slowly, but the state of charge (SOC) increases rapidly. As the number of cycles increases, the voltage platform will gradually shift upwards, and the SOH of the battery will decrease. As a unique electrochemical phenomenon in Li-S batteries, the gradual and small changes in voltage plateau are not conducive to quantitative analysis. Therefore, it is quantitatively analyzed by the following formulas:

$$\frac{\mathrm{d}Q}{\mathrm{d}V} = \frac{Q_t - Q_{t-1}}{V_t - V_{t-1}} \tag{6}$$

$$Q_t = \int_0^t I_t \mathrm{d}t \tag{7}$$

where Q_t is the battery capacity charge at time t; V_t is the voltage at time t; and I_t is the current at time t. Through the calculation of (6) and (7), the slowly changing area of the voltage plateau is converted into the peak value on the IC curve. This peak value corresponds to the extreme point on the $\mathrm{d}Q/\mathrm{d}V$ curve, and reflects the voltage plateau phenomenon. This approach establishes an intuitive connection between the external characteristics of the battery and the chemical reaction characteristics inside the battery. The obtained IC curve is shown in the black part of Fig. 3(a). The original IC curve has large noise, so the basic characteristics of the curve cannot be directly identified. Thus, it needs to be denoised and the Savitzky-Golay (S-G) filter is used, which is given as:

$$Y_j^* = \frac{\sum_{i=-m}^{i=m} C_i Y_{j+1}}{N} \tag{8}$$

where Y is the original sequence; Y^* is the filtered sequence; N represents the total number of sliding windows; j represents the position of the currently se-

lected filtering variable; C_i is the ith correlation coefficient of the sliding window, and the size of the sliding window is $2m+1$. Equation (8) is a basic first-order fitting, and is based on local polynomial least squares fitting in the time domain. One of its notable features is that it can filter out noise while preserving the shape and width of the signal. Additionally, it improves the smoothness of the curve and reduces the interference of noise, while different filtering degrees can also be achieved by changing the size of the sliding window.

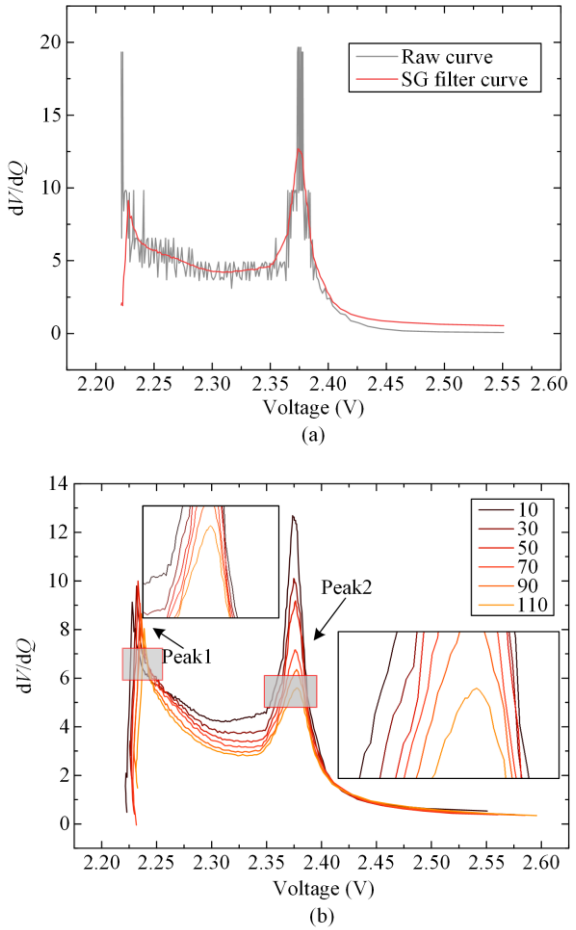

Fig. 3. The filtering effect of IC curve and comparison chart between different cycles. (a) IC curve before and after SG filter processing. (b) IC curves for different cycles at a charge rate of 1 C.

The curve obtained after applying SG filtering is illustrated in Fig. 3(b). In the IC curve shown in Fig. 3, the two slowly changing voltage plateaus are transformed into two distinct peaks, namely, Peak1 and Peak2. As the cycling progresses, the amplitudes of these two peaks gradually decrease, with Peak2 exhibiting a particularly noticeable decline. Additionally, the corresponding voltage of Peak2 undergoes a slight rightward shift as the cycling continues. Furthermore, the slopes of the curves on both sides of the peak gradually decrease as the cycling progresses. To conduct the correlation analysis, the characteristics are selected as health features. The scipy-find-peaks function in Python is employed, with the parameter distance set to 75, to extract the peaks corresponding to Peak1 and Peak2.

So far, a total of 9 groups of Li-S battery health features are extracted that may have high correlation, namely: charging voltage turning point, amplitude of Peak1, corresponding voltage of Peak1, left slope of Peak1, right slope of Peak1, amplitude of Peak2, corresponding voltage of Peak2, left slope of Peak2, and right slope of Peak2, and are calculated using Pearson correlation analysis, given as:

$$\rho(X,Y)=\frac{\mathrm{cov}(X,Y)}{\varepsilon_x\varepsilon_y} \tag{9}$$

where ρ represents the Pearson correlation coefficient; X and Y represent health characteristics and SOH, respectively; $\mathrm{cov}(X,Y)$ represents the covariance of the two; and $\varepsilon_x\varepsilon_y$ represents the product of the standard deviations of the two. If the absolute value of ρ is close to 1, it means that the correlation between the health feature and SOH is high. It is commonly accepted that a coefficient ρ with an absolute value exceeding 0.9 is indicative of a high-quality feature and can be used as the input feature of the neural network for inference training.

The scatter plot in Fig. 4 presents the calculation results for each health feature, using the data obtained at a charging rate of 1 C as an example. Notably, the correlation of the charging voltage turning point is 0.9995, indicating a strong relationship. Similarly, the voltage correlation of Peak2 is 0.992, the amplitude correlation of Peak2 is 0.975, the left slope correlation of Peak2 is 0.918, and the right slope correlation of Peak2 is −0.809. These five health features exhibit high correlations and are selected as input variables for the neural network.

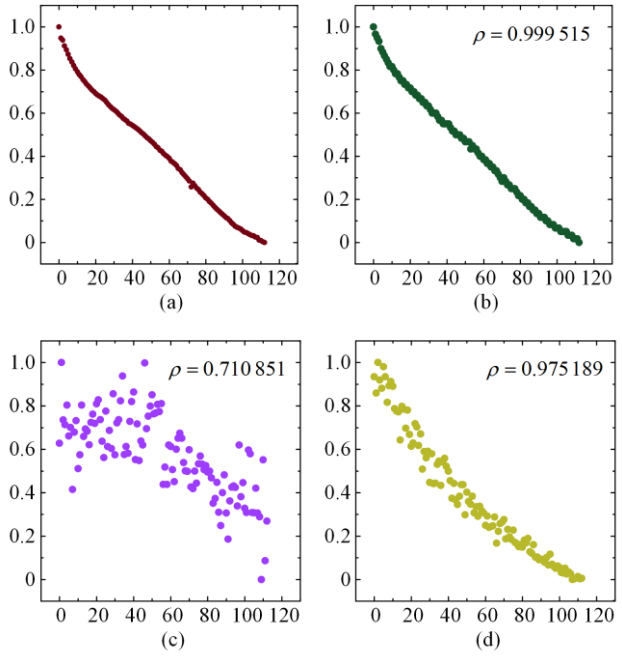

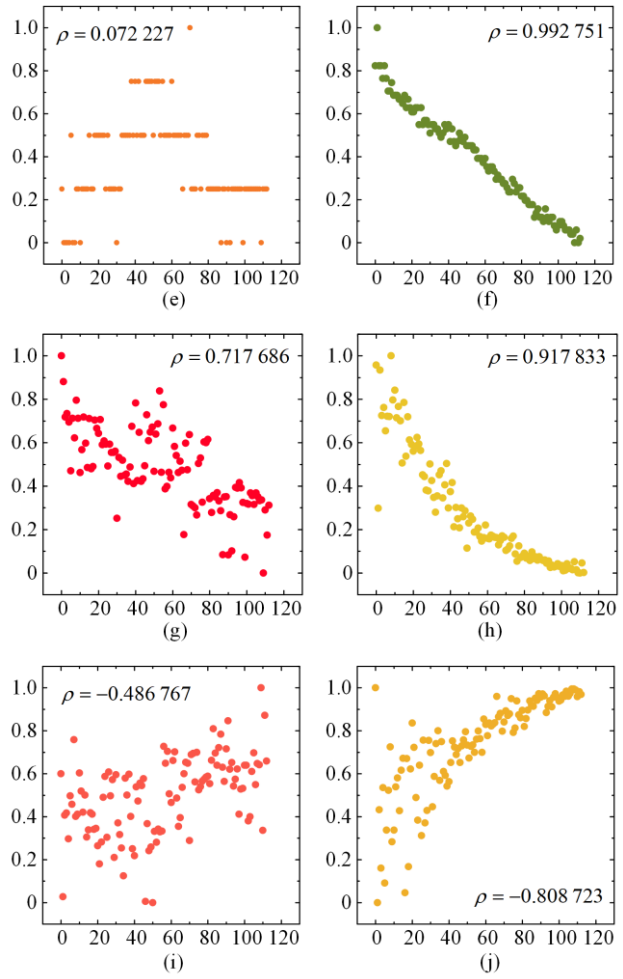

Fig. 4. Scatter plot of battery capacity and individual health characteristics at 1 C charge rate. (a) Charging voltage. (b) Voltage turning point. (c) The first peak of the IC curve. (d) The second peak of the IC curve. (e) IC curve first peak voltage. (f) IC curve second peak voltage. (g) Left slope of the first peak of the IC curve. (h) Left slope of the second peak of the IC curve. (i) Right slope of the first peak of the IC curve. (j) Right slope of the second peak of the IC curve.

IV. Methodology

A. Long Short-term Memory

Long short-term memory (LSTM) is a type of recurrent neural network (RNN) that represents an improvement over simple RNNs. When dealing with long input sequences in traditional neural network algorithms, a problem known as the gradient explosion or gradient disappearance may arise. This is also referred to as the long-term dependency problem. To overcome this challenge, gating mechanisms are introduced to enhance the performance of recurrent neural networks. LSTM and gated recurrent units (GRUs) are two prominent examples of such mechanisms. These gating mechanisms enable the network to selectively retain or discard information at each time step, to allow effective handling of long-term dependencies in the input sequence. By incorporating memory cells and various gates, LSTMs can capture and store relevant information over long periods, facilitating the modeling of complex temporal dependencies [35].

By way of example, Fig. 5 shows the detailed internal structure of the LSTM, in which it has three special network structures called 'gates'. The overall combined LSTM structure can effectively determine the forgetting or retention of information, as:

$$\boldsymbol{f}_t = \sigma_{\mathrm{g}}(\boldsymbol{W}_{\mathrm{f}}\boldsymbol{x}_t + \boldsymbol{U}\boldsymbol{h}_{t-1} + \boldsymbol{b}_{\mathrm{f}}) \tag{10}$$

$$\boldsymbol{i}_t = \sigma_{\mathrm{g}}(\boldsymbol{W}_{\mathrm{i}}\boldsymbol{x}_t + \boldsymbol{U}\boldsymbol{h}_{t-1} + \boldsymbol{b}_{\mathrm{i}}) \tag{11}$$

$$\boldsymbol{o}_t = \sigma_{\mathrm{g}}(\boldsymbol{W}_{\mathrm{o}}\boldsymbol{x}_t + \boldsymbol{U}\boldsymbol{h}_{t-1} + \boldsymbol{b}_{\mathrm{o}}) \tag{12}$$

$$\boldsymbol{C}_t = \boldsymbol{f}_t * \boldsymbol{C}_{t-1} + \boldsymbol{i}_t * \sigma_{\mathrm{c}}(\boldsymbol{W}_{\mathrm{c}} + \boldsymbol{U}\boldsymbol{h}_{t-1} + \boldsymbol{b}_{\mathrm{c}}) \tag{13}$$

$$\boldsymbol{h}_t = \boldsymbol{o}_t * \sigma_{\mathrm{c}}(\boldsymbol{C}_t) \tag{14}$$

where $\boldsymbol{x}_t$ represents input vector matrix; $\boldsymbol{f}_t$, $\boldsymbol{i}_t$, $\boldsymbol{o}_t$ and $\boldsymbol{C}_t$ represent the forget gate, input gate, output gate and update gate; $\boldsymbol{W}_{\mathrm{f}}$, $\boldsymbol{W}_{\mathrm{i}}$, $\boldsymbol{W}_{\mathrm{o}}$ and $\boldsymbol{W}_{\mathrm{c}}$ represent the input matrices of the forget gate, input gate, output gate, and update gate; $\boldsymbol{U}$ represents the output matrix; $\boldsymbol{b}_{\mathrm{f}}$, $\boldsymbol{b}_{\mathrm{i}}$, $\boldsymbol{b}_{\mathrm{o}}$, $\boldsymbol{b}_{\mathrm{c}}$ represent the input matrices of the forget gate, input gate, output gate and update gate; σ_{g} represents the sigmoid function; and σ_{c} represents the tanh function.

Equation (10) represents the forget gate, and combined with the current input x_t, the state C_{t-1} at the last moment, and the output h_{t-1} at the last moment, determines the memory to be deleted and retained. Equation (11) represents the input gate, and after the forget gate, the state C_t at the current moment is calculated according to x_t, C_{t-1} and h_{t-1}. Equation (12) represents the output gate, and after the input gate, the output h_t at the current moment is generated according to x_t, C_{t-1} and h_{t-1}. Equations (13) and (14) are the total formulae of the LSTM after combining the above gates.

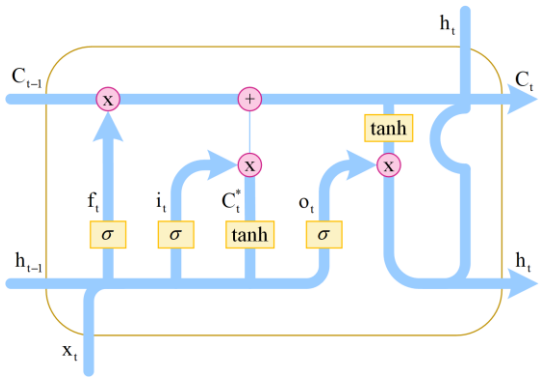

Fig. 5. LSTM structure.

B. Hyperparameters Optimization

The Adam optimizer is applied to the LSTM model to optimize the hyperparameters in the deep learning process. It is obtained by optimizing the momentum and

exponential moving average (EMA) of the gradient descent algorithm. The basic gradient descent algorithm is:

$$\theta_i^{t+1} \leftarrow \theta_i^t - \eta g_i^t \tag{15}$$

$$g_i^t = \frac{\delta L}{\delta \theta_i} |_{\theta=\theta^t} \tag{16}$$

where g represents the gradient; θ represents the network parameters; and η represents the update step size. Gradient descent updates the parameters in such a way that θ is updated with η as a step in the direction of decreasing gradient g. However, a common problem is that it is easy for gradient descent to fall into a local minimum. The way of momentum optimization is to consider the previous update state when θ is updated, to avoid following the sharp reduction of the gradient to obtain a local minimum. The specific formula is:

$$\theta_i^{t+1} \leftarrow \theta_i^t - \frac{\eta}{\sigma_i^t} g_i^t \tag{17}$$

where σ represents the parameter for adjusting the step size. The parameter σ is calculated with the root mean square (RMS) of all previous gradients in the Adagrad optimization algorithm. The RMSProp optimization algorithm increases the hyperparameter α to adjust the parameter σ as:

$$\sigma_i^t = \sqrt{\alpha(\sigma_i^t)^2 + (1-\alpha)(g_i^{t+1})^2} \tag{18}$$

Adjusting the size of α can change the weights of the previous and current gradients, thereby avoiding sudden changes in the gradient. The Adam optimization algorithm combines the advantages of both Adarad and RMSProp, integrates adaptive parameter calculation based on first-order moment mean, and fully uses bias to control θ and the step size of the update. It is a very popular algorithm, as shown in Fig. 6. In the calculation example of Li-S battery SOH, Adam's initial loss is large and there are fluctuations during the convergence process. However, because of its excellent convergence and adaptability, the loss quickly becomes lower than those of the Adarad and RMSProp optimizers, and it stabilizes after 100 epochs, which is more suitable for the prediction method proposed in this paper. The selected evaluation indicators are mean squared error (MSE) and mean absolute error (MAE), given as:

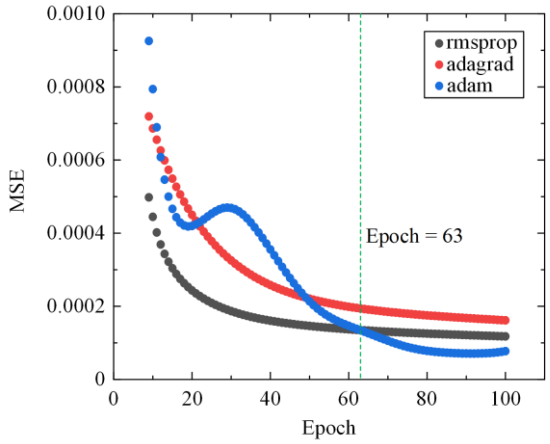

Fig. 6. Loss comparison of different optimizers.

$$MSE = \frac{1}{m}\sum_{i=1}^{m}(y_i - y_i')^2 \tag{19}$$

$$MAE = \frac{1}{m}\sum_{i=1}^{m}|y_i - y_i'| \tag{20}$$

where y_i' and y_i represent the predicted and actual capacities, respectively.

V. Experiments

Before the start of the experiments, in order to unify the size of various data and reduce the deep learning calculation, Z-score standardization is used to change all data to the range of [−1, 1], as:

$$\varphi = \frac{x-\mu}{\delta} \tag{21}$$

where x is the original data; μ is the mathematical expectation; δ is the standard deviation; and φ is the normalized data.

In this study, capacity estimation using the proposed LSTM model with Adam as the optimizer is performed on a notebook equipped with R75800H CPU and RTX3060 Laptop 6G GPU. LSTM data input is based on the three-dimensional data of (5, 6, 5), i.e., batch size is 5, time step is 6, and input feature is 6 (including capacity), while each epoch will start at a random starting point. Thirty-two sets of the above 3-dimensional arrays are added to the model to ensure the randomness of the training data and improve the generalizability of the model. Seventy-five recursions are performed for each epoch, with a learning rate of 0.001, whereas 100 epochs are performed in the training process, and the time required to complete an epoch is about 5 s. Three different training sets m of 20%, 40%, and 60% are used as input, and the remaining data is used as a validation set to input the existing LSTM model to complete the prediction. For comparison, the back propagation (BP) neural network, the RNN, and the LSTM network of non-ICA are also used with different training and quantities. Adam is used as the optimizer to implement the above four neural networks in Python.

To minimize the effect of random initialization of network parameters on the accuracy of capacity estimation, a Monte Carlo method is used to obtain 30 different capacity estimation results for each neural network of each test cell. The results are shown in Figs. 7(a)–(f). When predicting the SOH of the coated separators Li-S battery after 100 epochs, LSTM has the smallest overall prediction error while the BP neural network has the worst performance. The initial MSE of LSTM is larger, and BP and RNN perform better than LSTM in the first few epochs. However, because of the strong conver-

gence and adaptability of the Adam algorithm, the gradient is optimized in a very short time. The LSTM model without ICA has lower accuracy because of the lack of multi-dimensional features. It is proved that the improved LSTM algorithm proposed in this paper is very accurate for SOH estimation of Li-S batteries.

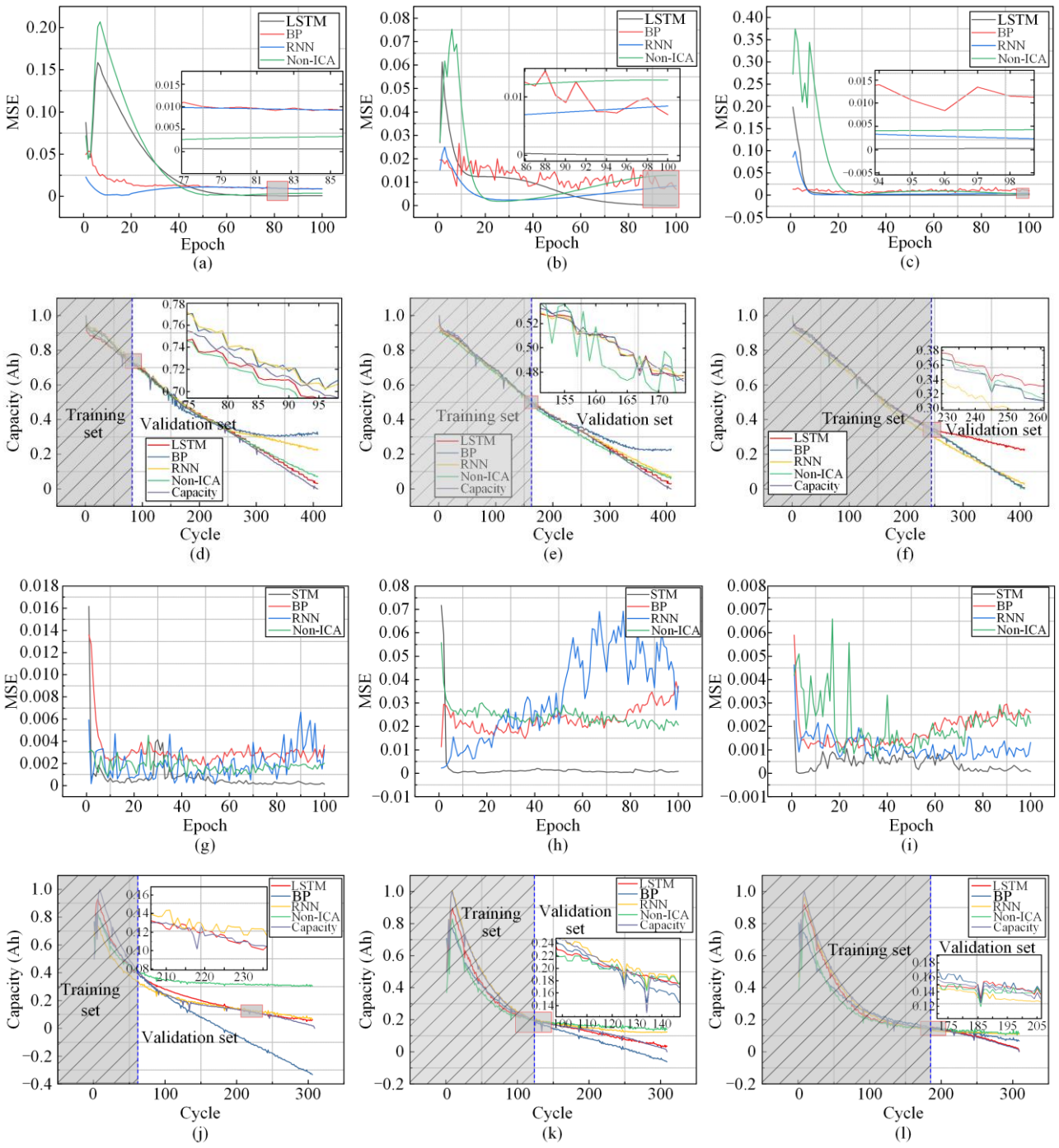

Fig. 7. (a) Validation set MSE of coated separator batteries when $m = 20\%$. (b) Validation set MSE of coated separator batteries when $m = 40\%$. (c) Validation set MSE of coated separator batteries when $m = 60\%$. (d) Capacity decay comparison curve when $m = 20\%$. (e) The capacity decay comparison curve when $m = 40\%$. (f) Capacity decay comparison curve when $m = 60\%$. (g) Validation set MSE for commercial separator batteries when $m = 20$. (h) Validation set MSE for commercial separator batteries when $m = 40$. (i) Validation set MSE for commercial separator batteries when $m = 60$. (j) Capacity decay comparison curve when $m = 20$. (k) The capacity decay comparison curve when $m = 40$. (l) Capacity decay comparison curve when $m = 60$.

Comparing the graphs in Figs. 7 (g)–(l), when m is 20%, 40% and 60%, LSTM still has the highest accuracy among the four neural networks, and the validation set errors have the minimum MSE of 0.054%, 0.013% and 0.011%, and the minimum MAE of 1.7%, 1.1% and 1.03%, respectively. The generalization performance of

the model at different m is the best. Even if the training set is small, there is no situation where other methods have small error in the training set and large deviation in the validation set. Figure 7 shows the prediction of the commercial separator Li-S batteries. The detailed MSE in different m conditions at different magnifications is shown in Table II. For Li-S batteries with two different separator materials, there are similar trends at different *m*, and LSTM is still the best prediction method. This proves that the LSTM model based on Adam optimization proposed in this paper is the best for SOH prediction of different types of Li-S batteries.

TABLE II
SOH PREDICTION ERROR MSE (%) TABLE OF FOUR NEURAL NETWORKS AT DIFFERENT CHARGING RATES

Battery	Coated seperators batteries						Commercial seperator batteries					
Train set length	20%		40%		60%		20%		40%		60%	
Type of error	MSE	MAE	MSE	MAE	MSE	MAE	MSE	MAE	MSE	MAE	MSE	MAE
ICA-LSTM	0.054	0.17	0.013	0.11	0.012	0.103	0.003	0.06	0.0021	0.046	0.0026	0.05
BP	0.84	0.85	0.68	0.78	0.45	0.68	0.083	0.28	0.096	0.31	0.11	0.34
RNN	0.097	0.42	0.24	0.51	0.13	0.36	0.01	0.094	0.023	0.17	0.018	0.11
LSTM (Non-ICA)	0.12	0.37	0.19	0.33	0.099	0.29	0.09	0.032	0.076	0.29	0.067	0.26

VI. CONCLUSION

In this study, an innovative approach for estimating the SOH of Li-S batteries is proposed. The method improves upon the existing LSTM model by considering both the external characteristics and internal reactions during battery charging and discharging. The health features are extracted using ICA, which are used as input data for the deep learning model. To enhance the performance of the LSTM model, critical hyperparameters are optimized using the Adam algorithm. The estimation results demonstrate that the proposed ICA-LSTM model outperforms other existing methods, such as BP, RNN, and LSTM (Non-ICA), particularly when a small training set is used. The experimental results reveal that the ICA-LSTM model achieves a prediction accuracy of MAE 4.6% and MSE 0.21% with three different training set lengths (20%, 40%, and 60%). This indicates that ICA significantly improves the accuracy of SOH estimation. The proposed method exhibits excellent generalizability, as it can provide high-precision SOH outputs for different Li-S batteries. The lightweight nature of the proposed model also enables easy implementation in offline hardware applications.

Overall, the study presents an innovative approach for Li-S battery SOH estimation, demonstrating the effectiveness of incorporating ICA and optimizing hyperparameters in the LSTM model. The results highlight the improved accuracy, generalization, and practicality of the method, making a contribution to advances in battery management systems.

ACKNOWLEDGMENT

Not applicable.

AUTHORS' CONTRIBUTIONS

Hao Zhang and Le Kang: writing original draft, methodology, conceptualization, software, investigation, formal analysis, manuscript review and editing. Hanlei Sun and Kai Wang: manuscript review and editing, conceptualization, methodology, supervision, project administration, funding acquisition. Yi Zhang and Licheng Wang: manuscript review and editing. All authors read and approved the final manuscript.

FUNDING

This work is supported by the Zhejiang Province Natural Science Foundation (No. LY22E070007) and National Natural Science Foundation of China (No. 52007170).

AVAILABILITY OF DATA AND MATERIALS

Please contact the corresponding authors for data material request.

DECLARATIONS

Competing interests: The authors declare that they have no known competing financial interests or personal relationships that could have appeared to influence the work reported in this article.

AUTHORS' INFORMATION

Hao Zhang works at the School of Materials Science and Engineering, Xi'an University of Architecture and Technology in Xi'an, Shanxi Province, China. His research interests include state assessment and life prediction of new energy storage devices, energy storage element.

Hanlei Sun graduated from School of Electrical Engineering, Qingdao University, Shandong Province, China. His research interests include state assessment and life prediction of new energy storage devices, distributed microgrid and energy storage.

Le Kang works at the College of Materials Science and Engineering, Xi'an University of Science and Tech-

nology, Xi'an, Shaanxi Province, China. His research interests include state assessment and life prediction of new energy storage devices, energy Internet.

Yi Zhang works at the School of Energy Sciences and Engineering, Nanjing Tech University, Nanjing, Jiangsu Province, China. His research interests include state assessment and life prediction of new energy storage devices, energy storage element.

Licheng Wang works at the School of Information Engineering, Zhejiang University of Technology, Hangzhou province, China. His research interests include state assessment and life prediction of new energy storage devices energy Internet.

Kai Wang works at the School of Electrical Engineering, Qingdao University, Shandong Province, China. He also works at Weihai Innovation Research Institute and Shandong Suoxiang Intelligent Technology Co., Ltd. His research interests include state assessment and life prediction of new energy storage devices, energy storage element, storage and conversion of new energy.

REFERENCES

[1] Y. Chen, C. Li, and S. Chen *et al.*, "A combined robust approach based on auto-regressive long short-term memory network and moving horizon estimation for state-of charge estimation of lithium-ion batteries," *International Journal of Energy Research*, vol. 45, no. 9, pp. 12838-12853, Mar. 2021.

[2] X. Han, L. Lu and Y. Zheng *et al*., "A review on the key issues of the lithium-ion battery degradation among the whole life cycle," *ETransportation*, vol. 1, Aug. 2019.

[3] X. Hu, Y. Che, and X. Lin *et al.*, "Battery health prediction using fusion-based feature selection and machine learning," *IEEE Transactions on Transportation Electrification*, vol. 7, no. 2, pp. 382-398, Aug. 2021.

[4] Y. Xie, H. Zhao and H. Chen *et al*., "Facile large-scale synthesis of core-shell structured sulfur@polypyrrole composite and its application in lithium-sulfur batteries with high energy density," *Applied Energy*, vol. 175, pp. 522-528, Aug. 2016.

[5] K. Liu, Y. Shang, and Q. Ouyang *et al*., "A data-driven approach with uncertainty quantification for predicting future capacities and remaining useful life of lithium-ion battery," *IEEE Transactions on Industrial Electronics*, vol. 68, no. 4, pp. 3170-3180, Mar. 2021.

[6] J. Hong, D. Lee, and Y. Yi *et al*., "Towards the swift prediction of the remaining useful life of lithium-ion batteries with end-to-end deep learning," *Applied Energy*, vol. 278, Nov. 2020.

[7] P. Ma, S. Cui, and M. Chen *et al*., "Review of family-level short-term load forecasting and its application in household energy management system," *Energies*, vol. 16, no. 15, Aug. 2023.

[8] X. Sun, Y. Zhang, and L. Wang *et al*., "Summary of health-state estimation of lithium-ion batteries based on electrochemical impedance spectroscopy," *Energies*, vol. 16, no. 15, Aug. 2023.

[9] C. Liu, Y. Zhang, and J. Sun *et al*., "Stacked bidirectional LSTM RNN to evaluate the remaining useful life of supercapacitor," *International Journal of Energy Research*, vol. 46, no. 3, pp. 3034-3043, Dec. 2022.

[10] X. Hu, L. Xu, and X. Lin *et al*., "Battery lifetime prognostics," *Joule*, vol. 4, no. 2, pp. 310-346, Feb. 2020.

[11] Y. Zhou, Z. Ma, and X. Shi *et al*., "Multi-agent optimal scheduling for integrated energy system considering the global carbon emission constraint," *Energy*, vol. 288, Feb. 2024.

[12] X. Li, J. C. Jiang, and L. Y. Wang *et al*., "A capacity model based on charging process for state of health estimation of lithium ion batteries," *Applied Energy*, vol. 177, pp. 537-543, Sept. 2016.

[13] H. Sun, D. Yang, and K. Wang *et al*., "A method for estimating the aging state of lithium-ion batteries based on a multi-linear integrated model," *International Journal of Energy Research*, vol. 46, no. 15, pp. 24091-24104, Sept. 2022.

[14] N. Ma, H. Yin, and K. Wang, "Prediction of the remaining useful life of supercapacitors at different temperatures based on improved long short-term memory," *Energies*, vol. 16, no. 14, Jul. 2023.

[15] M. Zhao, X. Chen, and X. Y. Li *et al*,, "An organodiselenide comediator to facilitate sulfur redox kinetics in lithium-sulfur batteries," *Advanced Materials*, vol. 33, no. 13, Apr. 2021.

[16] Z. Zheng, H. Ye, and Z. Guo, "Recent progress on pristine metal/covalent-organic frameworks and their composites for lithium-sulfur batteries," *Energy & Environmental Science*, vol. 14, no. 4, pp. 1835-1853, Apr. 2021.

[17] Y. Wei, H. Sun, and T. Zhang *et al*., "Study of inductively coupled fuel cell DMPPT converters," *Electrical Engineering*, Feb. 2024.

[18] J. Li, Z. Niu, and C. Guo *et al*., "Catalyzing the polysulfide conversion for promoting lithium sulfur battery performances: a review," *Journal of Energy Chemistry*, vol. 54, pp. 434-451, Mar. 2021.

[19] W. Wang, D. Yang, and Z. Huang *et al*., "Electrodeless nanogenerator for dust recover," *Energy Technology*, vol. 10, no. 12, Oct. 2022.

[20] J. Gao, D. Yang, and S. Wang *et al*., "State of health estimation of lithium-ion batteries based on Mixers-bidirectional temporal convolutional neural network," *Journal of Energy Storage*, vol. 73, Oct. 2023.

[21] X. Yu, Y. Shang, and L. Zheng *et al*., "Application of nanogenerators in the field of acoustics," *ACS Applied Electronic Materials*, vol. 5, no. 9, pp. 5240-5248, Oct. 2023.

[22] Y. Liu, L. Wang, and D. Li *et al*., "State-of-health estimation of lithium-ion batteries based on electrochemical impedance spectroscopy: a review," *Protection and Control of Modern Power Systems*, vol. 8, no. 3, pp. 1-17, Jul. 2023.

[23] X. Yu, T. Ai, and K. Wang, "Application of nanogenerators in acoustics based on artificial intelligence and machine learning," *APL Materials*, vol. 12, no. 2, Feb. 2024.

[24] X. Liang, J. Yun, and Y. Wang *et al.*, "A new high-capacity and safe energy storage system: lithi-

um-ion sulfur batteries," *Nanoscale*, vol. 11, no. 41, pp. 19140-19157, Nov. 2019.

[25] Y. Chen, T. Wang, and H. Tian *et al.*, "Advances in lithium-sulfur batteries: from academic research to commercial viability," *Advanced Materials*, vol. 33, no. 29, Jul. 2021.

[26] P. Chen, Z. Wu, and T. Guo *et al.*, "Strong chemical interaction between lithium polysulfides and flame-retardant polyphosphazene for lithium-sulfur batteries with enhanced safety and electrochemical performance," *Advanced Materials*, vol. 33, no. 9, Mar. 2021.

[27] W. Li, N. Sengupta, and P. Dechent *et al.*, "Online capacity estimation of lithium-ion batteries with deep long short-term memory networks," *Journal of Power Sources*, vol. 482, Jan. 2021.

[28] X. Hu, J. Jiang, and D. Cao *et al.*, "Battery health prognosis for electric vehicles using sample entropy and sparse bayesian predictive modeling," *IEEE Transactions on Industrial Electronics*, vol. 63, no. 4, pp. 2645-2656, Apr. 2016.

[29] Z. Yi, Z. Chen, and K. Wang *et al.*, "Sensing as the key to the safety and sustainability of new energy storage devices," *Protection and Control of Modern Power Systems*, vol. 8, no. 1, pp. 1-22, Apr. 2023.

[30] H. Zhang, J. Gao, and L. Kang *et al.*, "State of health estimation of lithium-ion batteries based on modified flower pollination algorithm-temporal convolutional network," *Energy*, vol. 283, Aug. 2023.

[31] L. Wang, L. Xie, and Y. Yang *et al.*, "Distributed online voltage control with fast PV power fluctuations and imperfect communication," *IEEE Transactions on Smart Grid*, vol.14, no.5, pp. 3681-3695, Sept. 2023.

[32] Y. Guo, P. Yu, and C. Zhu *et al.*, "A state-of-health estimation method considering capacity recovery of lith ium batteries," *International Journal of Energy Research*, vol. 46, no. 15, pp. 23730-23745, Sep. 2022.

[33] N. Shateri, D. J. Auger, and A. Fotouhi *et al.*, "An experimental study on prototype lithium-sulfur cells for aging analysis and state-of-health estimation," *IEEE Transactions on Transportation Electrification*, vol. 7, no. 3, pp. 1324-1338, Aug. 2021.

[34] V. Knap, D. Auger, and K. Propp *et al.*, "Concurrent real-time estimation of state of health and maximum available power in lithium-sulfur batteries," *Energies*, vol. 11, no. 8, Aug. 2018.

[35] H. Sun, J. R. Sun, and K. Zhao *et al.*, "Data-driven ICA-Bi-LSTM-combined lithium battery SOH estimation," *Mathematical Problems in Engineering*, vol. 2022, Mar. 2022.

[36] C. Zhang, Y. He, and L. Yuan *et al.*, "Capacity prognostics of lithium-ion batteries using EMD denoising and multiple kernel RVM," *IEEE Access*, vol.5, pp. 12061-12070, Oct. 2017.

[37] S. Wang, F. Wu, and P. Takyi-Aninakwa *et al.*, "Improved singular filtering-Gaussian process regression-long short-term memory model for whole-life-cycle remaining capacity estimation of lithium-ion batteries adaptive to fast aging and multi-current variations," *Energy*, vol. 284, Dec. 2023.

[38] S. Wang, Y. Fan, and S. Jin *et al.*, "Improved anti-noise adaptive long short-term memory neural network modeling for the robust remaining useful life prediction of lithium-ion batteries," *Reliability Engineering & System Safety*, vol. 230, Feb. 2023.

[39] Z. Yang, X. Zhang, and Z. Li *et al.*, "Interlinked carbon nanocages-coated separator as an efficient trap for soluble polysulfides in a lithium-sulfur battery," *Energy & Fuels*, vol. 35, no. 23, pp. 19843-19848, Jul. 2021.